Contract No:

This document was prepared in conjunction with work accomplished under Contract No. DE-AC09-08SR22470 with the U.S. Department of Energy (DOE) Office of Environmental Management (EM).

Disclaimer:

SRNL-STI-2014-00275

DEVELOPMENT AND CHARACTERIZATION OF NANOMATERIALS FOR ZINC VAPOR CAPTURE

Paul S. Korinko and Simona E. Murph

Keywords: Zinc Vapor, Nanoparticles, Characterization, Getters

For publication in the proceedings from

TMS 2015 144th ANNUAL MEETING & EXHIBITION

MARCH 15-19, 2015 • Orlando, FL, USA

DEVELOPMENT AND CHARACTERIZATION OF NANOMATERIALS FOR ZINC VAPOR CAPTURE

Paul S. Korinko[1] and Simona E. Hunyadi Murph[1]
[1]Savannah River National Laboratory, Aiken, SC 29808

Keywords: Zinc Vapor, Nanoparticles, Characterization, Getters

Abstract

To address a radiological contamination event, a materials and process project was initiated. During the course of this project, processes and materials were developed that successfully captured zinc vapors physically and chemically, respectively. However, the physical traps were placed in an undesirable area and it was determined that the chemically captured zinc reactions was reversible. Consequently, advanced nanomaterials are being developed to capture zinc vapors. The current state of the art of the science and engineering of these materials and their efficacy for zinc capture and retention is discussed in this paper.

Introduction

A radiological contamination [1] event several years ago, resulted in the planning and execution of a development program to capture and retain zinc vapors [2]. The initial approach resulted in physical [3] then chemical trapping methods for zinc capture [4]. During a simulated process evolution, it was observed that copper–tin alloy (bronze) zinc getters were prone to reversible reactions [5]. Dezincification is a known issue for brasses especially at high temperatures under vacuum conditions, but the temperature range of interest for this application is lower than what has typically been described [6, 7].

Due to the reversible zinc getter behavior for bronze, an investigation into using materials of higher temperature, and presumed higher thermal stability was conducted. Bulk cobalt, which is expected to react with zinc but not with hydrogen [8], was initially used but the zinc vapors physically deposited onto the substrate and no alloying occurred. Consequently, the concept of using nanomaterials of suitable composition, reactivity and process stability evolved. Nanomaterials exhibit unique properties due to their large surface area and quantum size effects [9, 10]. It was expected that they would be able to react at relatively low homologous temperatures, would coarsen due to the reactions, and would be more stable than the bronze materials that were initially tested. This paper presents preliminary results for gold, cobalt, and gold-cobalt alloys nanomaterials that were grown on stainless steel wool trap material.

Experimental

A total of seven different nanomaterials were grown on Type 316L stainless steel wool (SS-W), the material currently used for the process lid. The as-received stainless steel wool (control) was characterized using a Keyence VR 3000 profilometer and scanning electron microscopy (SEM).

All of the nanomaterials were grown onto substrates of SS-W that were nominally 50 mm diame-

ter x 10 mm diameter pads. The nanomaterials were grown from aqueous solutions using conditions that would produce the desired deposit size and shape. Gold and cobalt nanoparticles were prepared by a citrate reduction approach [9-11] in the presence of SS-W. With this synthesis, $1.25x10^{-4}$M Au^{3+} was heated to boiling and 1 wt % sodium citrate solution was added. The boiling was continued until the solution turned ruby red, indicating the formation of gold nanoparticles. Gold cobalt alloys nanoparticles were prepared by a similar procedure by reducing a mixture of $1.25x10^{-4}$M Au^{3+} and $1.25x10^{-4}$M Co^{2+}. Core-shell Au-Co nanostructures were prepared in two steps (a) synthesis of Au (0) nanosphere core seeds and (b) Co shell by the procedure described above. The resulting nanoparticles were purified by three-five steps washing in deionized water.

The nanoparticle (NP) deposits were characterized using scanning electron microscopy (SEM), energy dispersive X-ray analysis (EDX) and EDX elemental mapping to elucidate their morphology, topography and composition. The NP optical properties were evaluated by UV-Vis spectroscopy. The adhesion of the NP deposit to the SS-W was tested using an ultrasonic cleaner and an aqueous solution using fixed time increments. The liquid was analyzed using inductively coupled plasma atomic emission spectroscopy (ICP-AES) to determine the amount of the deposit that was removed. ICP-AES experiments were also performed to quantify the amount of metals present on the support (Zn, Co, Au). This technique allowed quantification of chemical composition of our colloids and accurate Zn capturing/loading information.

Samples were exposed to zinc vapor from a high vacuum thermal deposition apparatus. The system is comprised of an all metal seals and Conflat™ flanges. The samples were supported on perforated metal with a stack of up to four samples being exposed during one exposure. A bronze pellet was included in the exposure as an experimental control and to verify that the deposition apparatus operated correctly. The zinc vaporization and filter temperature conditions, 350°C for both and an initial vacuum pressure of approximately 5 x 10^{-6} Torr, used were consistent with previous work [5].

Results

The SS-W was examined optically using the Keyence VR3000 with the results shown in Figure 1. Note the roughened surface condition of the wire filament. The nominal diameter of the wires is 50 µm. The surface roughness was also measured and it indicates a roughness of 5.44 Ra.

The nanoparticle's optical properties were evaluated by UV-Vis spectroscopy. In deionized water, the gold nanoparticles display the characteristic peak at around 525 nm that corresponds to the plasmon band (collective oscillation of electrons) for spherical gold nanoparticles while the cobalt nanospheres have

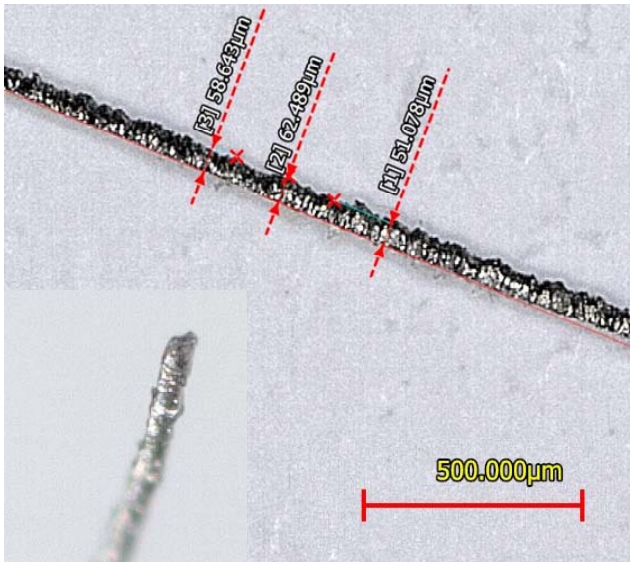

Figure 1. Appearance of a SS-W wire filament showing the surface condition and the shape.

a plasmon band around 384 nm [9-11]. The UV-Vis spectra of the bimetallic Au-Co nanostructures differ from the monometallic colloids. A continuous red shift of the Au nanospheres plasmon band, originally at approximatively 525 nm, confirms the formation of bimetallic Au-Co colloids with a plasmon band around 533 nm [10-12]. The nanoparticle composition and chemistry can be monitored using the solution color (inset photo) Figure 2.

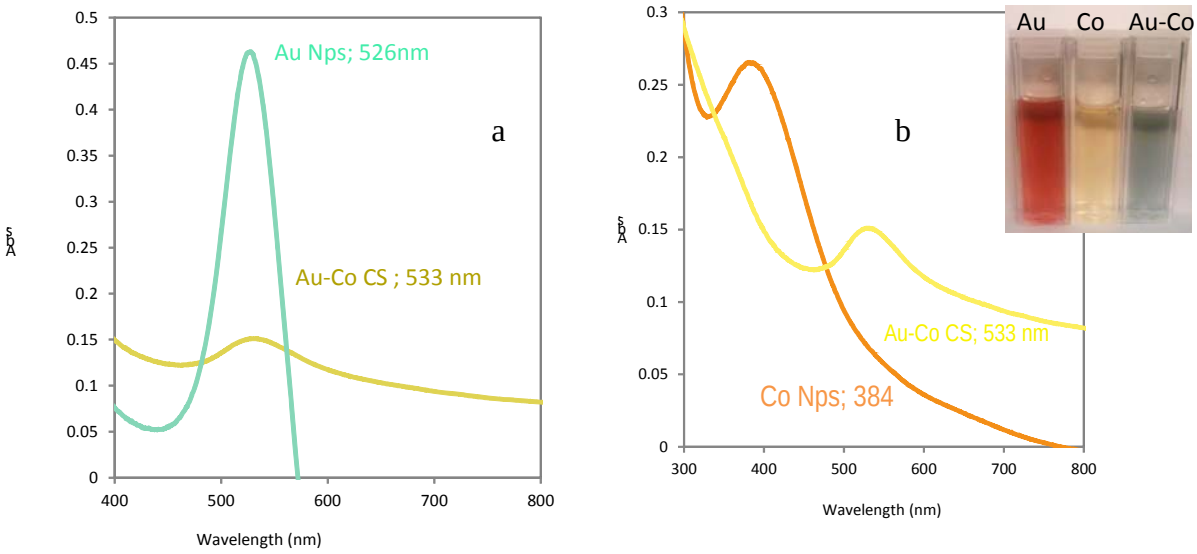

Figure 2. (a) Appearance of the solution and (b) the UV-Vis spectra for Au and Au-Co (c) the UV-Vis spectra for Co and Au-Co.

Nanoparticles of Au were grown onto SS-W using the described procedures. The Au NPS as-deposited condition of the wire is shown in Figure 3. Two different morphologies are formed on the SS-W surfaces, nanospheres and spherical nanoclusters. The nanospherical particles are nominally 26 nm in diameter (30%) while the spherical nanoclusters, formed by agglomeration of the 26 nm nanospheres, are approximatively 78 nm (70%) in diameter with a relative spacing of 100 nm. SEM images show that the nanoparticles are distributed over the entire wire surfaces. Despite the surface condition shown for the wires, the particles appear to be randomly deposited on the wire surface. This result is not surprising since the SS-W surface is non-uniform. The SS-W has a surface roughness of 5.44 RA. Figure 3 shows a multitude of valleys, steps and crevices that may be critical for random nanoparticle deposition.

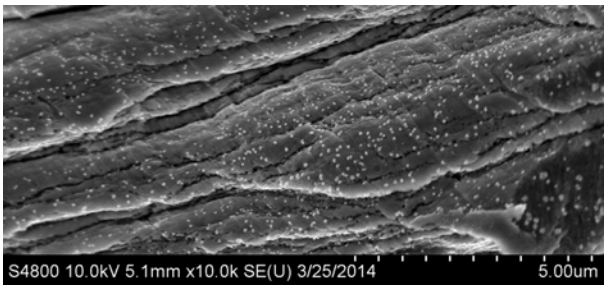

Figure 3. Gold nanoparticles deposited onto the 50 micron SS-W wires. Note the small size and random distribution.

Three Au-Co alloys and alloy-types with various quantities and morphologies of Au and Co were also deposited on SS-W. One of the Au-Co alloy samples is shown in Figure 4. In general, these nanomaterials also exhibit random particle deposition with a size range of 30 to 220 nm in diameter, for single and agglomerated particles, respectively. Selected sample particle size ranges are listed in Table I.

Single samples of Au, Co, and Au-Co alloy functionalized SS-W were exposed to zinc vapor using previously established conditions [5]. The typical thermal and pressure profiles observed are indicated in Figure 5. The filter reaches the target temperature before the zinc is heated so that the zinc vapor can be captured at the desired temperature. Previous work indicated that low temperatures result in physically trapped zinc with inadequate adhesion [5].

Visual examination of the bare and nanomaterial treated SS-W exposed to zinc did not reveal any change in color as is typically observed for the bronze pellets which are initially orange (bronze) colored and change to a golden tint (brass) after zinc alloying, as shown in Figure 6 for SS-W and bronze pellets, respectively. There may be a slight change in the sheen of the SS-W indicated by the photos, but this difference may simply be due to changes in lighting between the photos.

EDX microanalysis of Au, Co, and Au-Co nanomaterials before and after Zn exposure was performed to evaluate nanomaterial composition of mono and bimetallic colloids with representative data presented in Figure 7.

All of the zinc exposed samples were examined using SEM and EDX to characterize how effective the nano-materials were as zinc getters. SEM analysis was needed since mass changes were unmeasurable due to wire breakage, wire loss, and moisture evaporation during weighing. The control SS-W sample was examined after zinc exposure and no zinc was detected. The results are shown in Figure

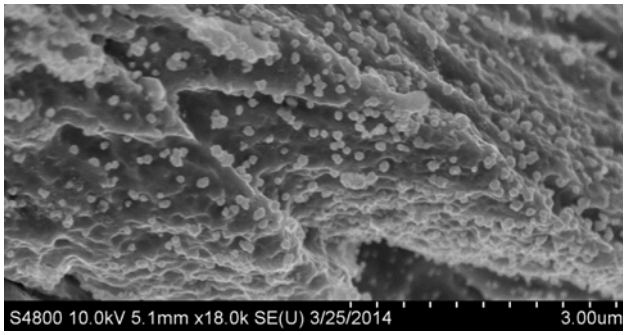

Fig.4. This is an image of the as deposited Au-Co (#1) on the stainless steel wire. The particles are generally randomly oriented a spherical shape. There are some agglomerated particles as well.

Table I. Particle size distribution of the gold-cobalt alloys and alloy-type nanostructures.

Au-Co Alloy (nm)	Au-Co CS (nm)	Au-Co-Co ACS (nm)
30	30	42
128	80	71
		101
		220

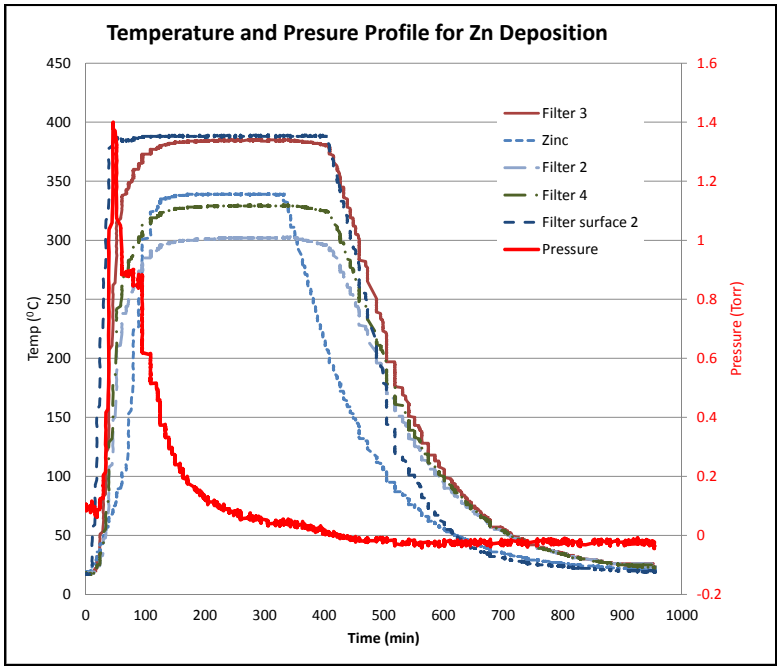

Figure 5. Typical zinc thermal and pressure response.

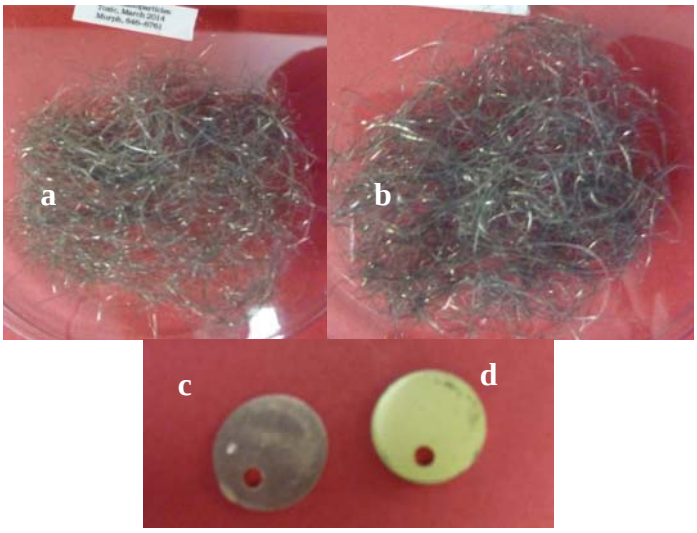

Figure 6. Appearance of SS-W before (a) and after (b) zinc exposure and typical bronze pellets before (c) and (d) after zinc exposure.

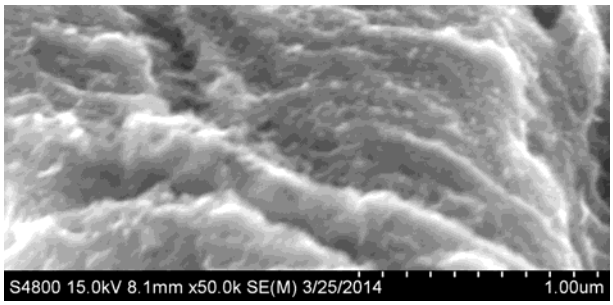

a

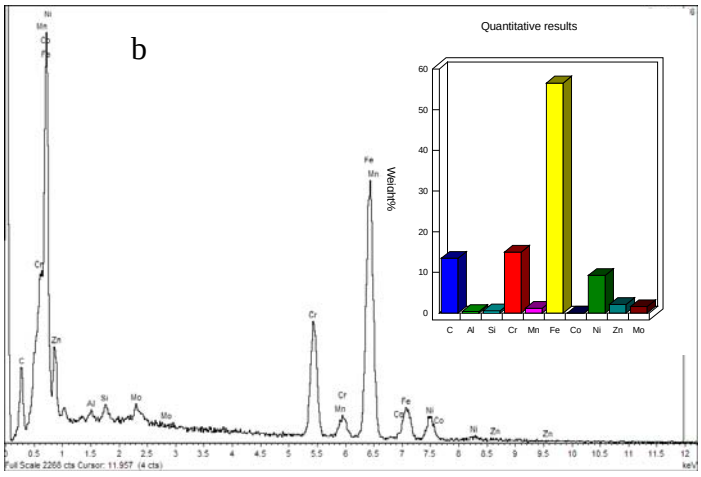

Figure 7 (a) Appearance of nano-cobalt (Co CT #4) deposited on SS-W after zinc exposure; (b) showing zinc was present on the sample, composition indicated in Table II.

8. Semi-quantitative analysis was conducted on the sample as well as X-ray dot mapping. The EDX mapping analysis demonstrates the accurate location of the elements of interest: Au, Co and Zn. The chemical analyses for the zinc exposed samples are listed in Table II.

Figures 7a, 9, and 10a show the surface appearance of Au, Co, and Au-Co alloy samples, respectively, after zinc exposure. The samples all exhibit coarsening of the nanodeposit getters. The relative size changes are shown in Figure 12. All of the samples that were treated with nanomaterials were effective at gettering the zinc vapor at a nominal temperature of 350°C. The Zn content ranged from ~2.5 to ~7 wt %. This range has little overall significance, since the areas examined include a substantial amount of non-treated SS-W as well as the beam interaction volume as indicated by the X-ray dot maps. These results clearly show that all the nanomaterials capture zinc while the control SS-W remains inert; a result that is consistent with the practical experience [1].

More rigorous metal quantification was conducted using ICP-AES. All nanoparticles deposited onto solid supports were sonicated at regular time intervals (10 min, 30 min and 60 min) in deionized water. The resulting aqueous colloids were dissolved in aqua regia and subjected to ICP-AES in order to quantify the amount of metals present. Representative data are presented in Figure 12.

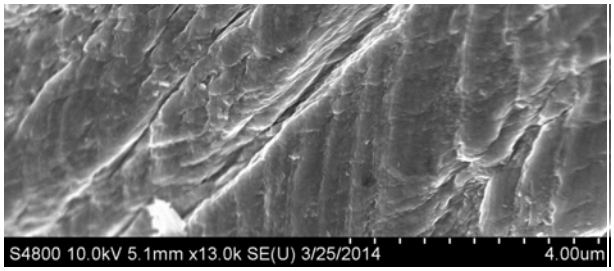

Figure 8. Appearance of baseline SS-W after zinc exposure. Zinc was not detected on the surfaces as indicated in Table 2.

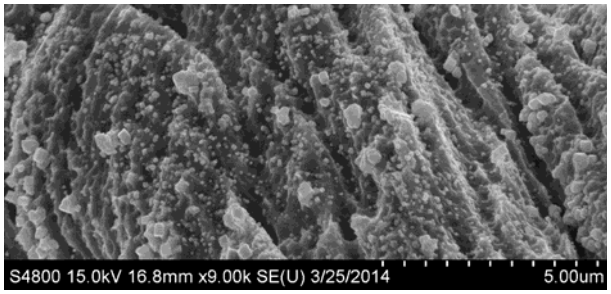

Figure 9. Appearance of nano-gold deposited on SS-W after zinc exposure. Zinc was present on the sample as indicated in Table 2.

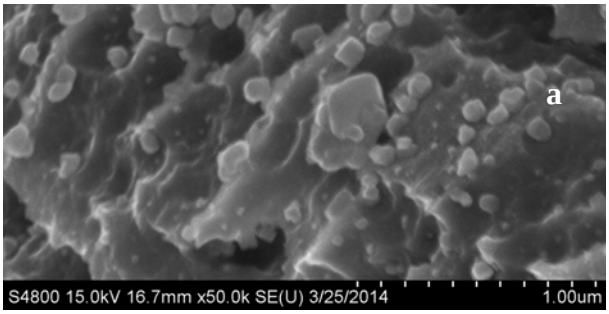

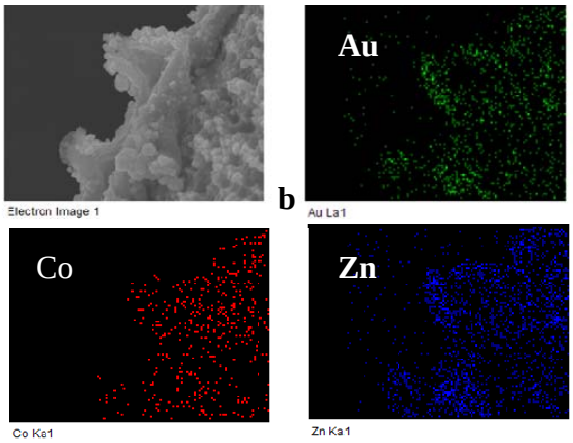

Figure 10. (a) Appearance of nano-gold-cobalt alloy deposited on SS-W after zinc exposure; and (b) X-ray dot map of the deposit, composition indicated in Table II.

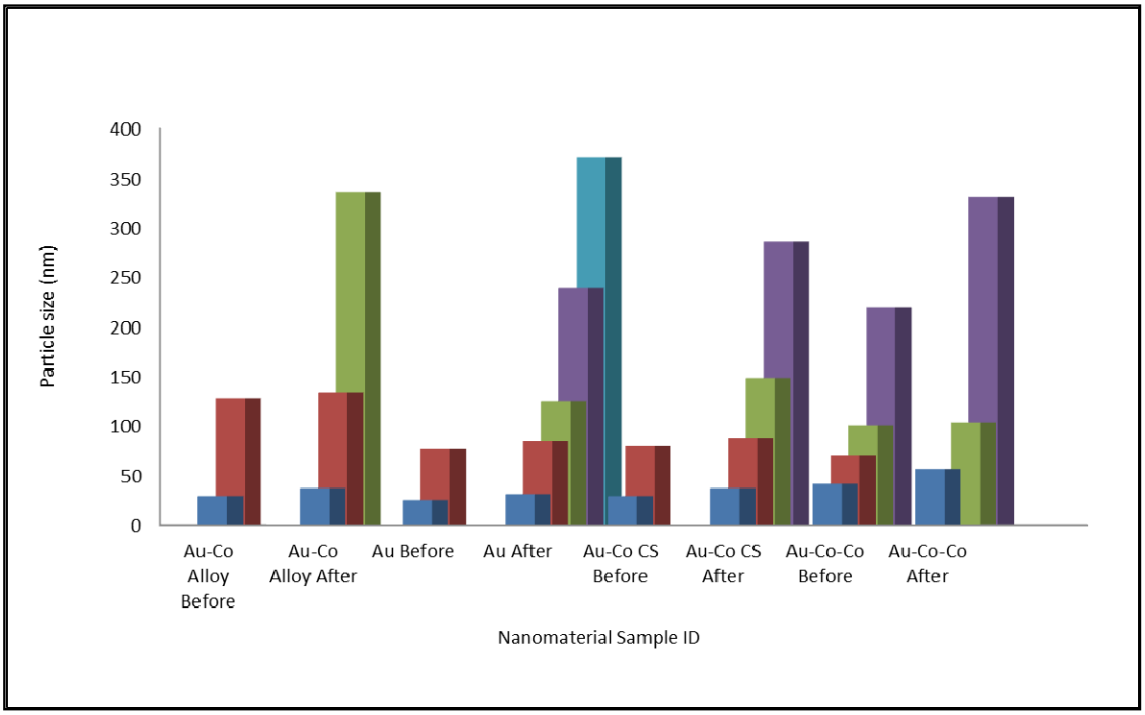

Figure 11. Zinc exposure increased the size of the particles observed

Table II. Composition of deposits based on semi-quantitative X-ray Energy Dispersion Analysis.

ID	#0	#1	#2	#3	#3	#4	#5	#5
Element	Wt %	Wt %	Wt %	Wt %	Wt %	Wt %	Wt %	Wt %
C K	10.98	11.16	24.62	5.53	56.03	4.55	14.75	53.57
O K	NM	2.85	4.01	0.89	5.01	NM	2.29	7.73
Al K	NM	0.36	NM	0.18	0.17	0.3	45.31	NM
Cr K	16.25	11.84	12.11	15.81	5.13	17.07	4.58	6.34
Mn K	NM	3.71	NM	1.05	NM	0.95	0.68	NM
Fe K	66.01	49.97	40.44	58.4	18.33	62.76	16.69	21.5
Co K	NM	NM	NM	0.04	0.07	0.33	0.08	0.01
Ni K	6.76	7.6	5.52	9.53	2.85	9.11	2.56	2.96
Zn L	NM	5.74	7.22	5.79	5.71	2.49	3.51	3.51
Au M	NM	6.77	6.08	2.78	6.71	NM	5.96	4.39
Mo L	NM	NM	NM	NM	NM	2.17	NM	NM
Si K	NM	NM	NM	NM	NM	0.27	NM	NM
Cu L	NM	NM	NM	NM	NM	NM	3.58	NM
Totals	100	100	100	100	100	100	100	100

#0 Control SSW; #1 Au-Co alloy; #2 Au; #3 Au-Co Coreshell; #4 Co CT; #5 Au-Co Co coreshell

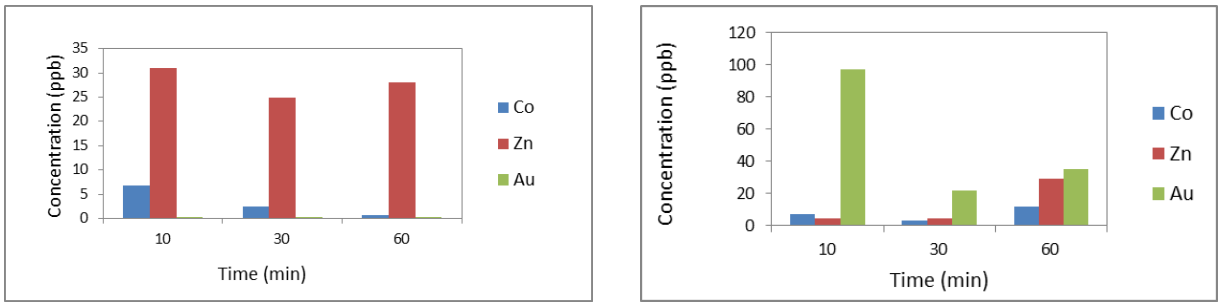

Figure 12. ICP-AES data on Au-Co colloids (a) before Zn exposure and (b) after Zn exposure.

Summary and Conclusions

Nanoparticles can be grown on stainless steel wool. The rough surface morphology and topography of the 50 nm SS-W lends itself to random particle growth with a narrow size distribution and some agglomeration.

Zinc is preferentially deposited onto SS-W that has been treated with nanoparticles. The zinc vapor does not deposit and grow on the control SS-W. Preliminary results indicate that Au nanoparticles are superior to Co and Au-Co alloys.

The composition of the nanoparticles after zinc exposure consists of 2.5-7% zinc, but the sample volume contains a significant amount of the SS-W substrate based on the high iron and chromium contents.

Acknowledgements

The authors would like to acknowledge Todd Woodsmall and Bob Snyder of the Savannah River Tritium Enterprise for providing funding for this work under contract DE-AC09-08SR22470. They would also like to recognize the contributions of summer interns Ansely Summer, Rebecca Lewis, and Jacqueline Polz.

References

1. Paul S. Korinko and Michael H. Tosten, "Analysis of Zinc 65 Contamination After Vacuum Thermal Process", *Journal of Failure Analysis and Prevention,* 13 (4), (2013), 389-395.
2. Paul S. Korinko, Andrew J. Duncan and Kevin J. Stoner, "Methods of Preventing the Spread of Zinc Contamination During Vacuum Processing", *Journal of Failure Analysis and Prevention,* 14 (1) (2014), 113-121.
3. Paul S. Korinko, "Zinc 65 Sequestration Path Forward" Correspondence/SRNL-L4410-2013-00004, Feb. 25, 2013.
4. M. Golyski and P. Korinko, "Effect of Thermal Processes on Copper-Tin Alloys for Zinc Gettering", SRNL Report/SRNL-STI-2013-00625, Oct. 8, 2013.
5. P. Korinko, "Effectiveness of Copper and Bronze for Zinc Capture", SRNL Report/SRNL-STI-2012-00616, Oct. 2012.
6. J.S. Broadley and E. Bevitt, "Evaporation of Zinc from Solid Solutions", United Kingdom Atomic Energy Authority, Risley, Warrington, Lancashire, March 1954.
7. I. Itoh and T. Hikage, "Dezincification Mechanism of Brass in Vacuum at High Temperature", *Trans Japan Institute of Metals*, 17 (1976) 165-169.
8. P.S. Korinko, "Zinc Mitigation Interim Report–Thermodynamic Study", SRNL Report/SRNL-STI-2010-00473, Dec 17, 2010.
9. S.E. Hunyadi Murph, et al., "Metallic and Hybrid Nanostructures: Fundamentals and Applications", in *Applications of Nanomaterials*, Vol.4: Nanomaterials and Nanostructures, Studium Press LLC, Houston TX, USA. 2012.
10. S.E. Hunyadi Murph, et al., "Tuning of Size and Shape of Au-Pt Nanocatalyst for Direct Methanol Fuel Cells" *J. Nanoparticle Research*, 13, (2011), 6347-6364.
11. S.E. Hunyadi and C.J. Murphy, "Synthesis and Characterization of Silver-Platinum Bimetallic Nanowires and Platinum Nanotubes", *Journal of Cluster Science,* 2009, 20, 319-330.
12. S.E. Hunyadi and C.J. Murphy, "Bimetallic Silver-Gold Nanowires: Fabrication and Use in Surface-Enhanced Raman Scattering" *J. Mater. Chem*.; Special Issue: Anisotropic Nanoparticles 16, (2006), 3929 - 3935.